In the format provided by the authors and unedited.

Attosecond coupled electron and nuclear dynamics in dissociative ionization of H₂

L. Cattaneo [1]*, J. Vos[1], R. Y. Bello[2], A. Palacios[2,3], S. Heuser[1], L. Pedrelli[1], M. Lucchini [1,7], C. Cirelli[1,4], F. Martín[2,5,6] and U. Keller [1]

---

[1]Physics Department, ETH Zurich, Zurich, Switzerland. [2]Departamento de Química, Módulo 13, Universidad Autónoma de Madrid, Madrid, Spain. [3]Institute for Advanced Research in Chemical Sciences (IAdChem), Universidad Autónoma de Madrid, Madrid, Spain. [4]Empa – Swiss Federal Laboratories for Materials Science and Technology, Dübendorf, Switzerland. [5]Instituto Madrileño de Estudios Avanzados en Nanociencia (IMDEA-Nanociencia), Madrid, Spain. [6]Condensed Matter Physics Center (IFIMAC), Universidad Autónoma de Madrid, Madrid, Spain. [7]Present address: Department of Physics, Politecnico di Milano, Milano, Italy. *e-mail: claura@phys.ethz.ch

Attoecond coupled electron and nuclear dynamics in dissociative ionization of H$_2$

Supplementary Information

1. Molecular frame and Kinetic Energy Release (KER) definitions

As illustrated in the inset of Fig. 1b, the angle between the dissociating H_2^+ molecule with respect to the XUV polarization axis, β, can be obtained by measuring the vector momenta $\vec{p}_{H^+}^{LF}$ of the H^+ ion and $\vec{p}_{e^-}^{LF}$ of the electron in the laboratory frame (LF) and calculating the corresponding H^+ momentum $\vec{p}_{H^+}^{MF}$ in the molecular frame (MF) as follows:

$$\vec{p}_{H^+}^{MF} = \vec{p}_{H^+}^{LF} + \frac{1}{2}\vec{p}_{e^-}^{LF} \quad (1)$$

Then the β angle can be calculated:

$$\beta = \tan^{-1}\frac{\sqrt{\left(\vec{p}_{H^+,x}^{MF}\right)^2 + \left(\vec{p}_{H^+,y}^{MF}\right)^2}}{\vec{p}_{H^+,z}^{MF}} \quad (2)$$

where $\vec{p}_{H^+,x,y,z}^{MF}$ are the x,y,z-component of the H^+ momentum in the MF. In the present work only the dissociative photoionization processes are considered, i.e. filtering the acquired particles in accordance with the time-of-flight of the H$^+$ fragment ion.

The KER, that is the sum of the kinetic energies of the ion and neutral fragments formed by the dissociation of H_2^+, plays a fundamental role in order to fully understand the dissociative ionization dynamics under investigation.

Although neutral fragments (H) are not detected, the measured momenta of the coincident ion-electron (H^+ and e^-) pair allow reconstructing the missing H momentum and thus its kinetic energy. Therefore, the KER can be expressed as the sum of the neutral and fragment ion:

$$KER = E_{kin}^{H^+} + E_{kin}^{H} = \frac{\left[p_{H^+}^{MF}\right]^2 + \left[\left(p_{H^+}^{LF} + p_{e^-}^{LF}\right)_H^{MF}\right]^2}{2m_H} \quad (3)$$

where m_H is the hydrogen atomic mass.

2. XUV only correlation diagrams

Figure 1_represents the time-integrated dissociative ionization probability of H$_2$ as a function of the KER (H$^+$ + H) and electron kinetic energy when only the XUV field is present, distinguishing between β$_{//}$ and β$_\perp$.
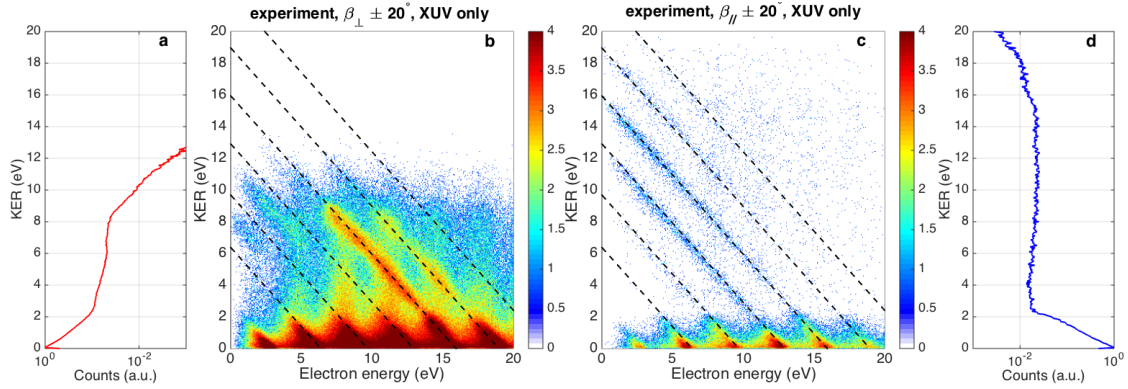
Figure 1: Correlation diagrams XUV only. Dissociative ionization probability as a function of the kinetic energy release (KER) and electron kinetic energy selecting on (a,b) $\beta_\perp$, cone 70-110°, and (c,d) $\beta_{//}$ (cone 0-20° and 160-180°), when only the XUV APT is present. Panels a) and d) represent the KER integrated over the electron kinetic energy.

3. IR-fluencies estimation

Figure 2 represents the normalized nuclear fragments yield (H$^+$ + H) as a function of KER for different data sets. Each set has been measured with a different IR intensity tuned by means of an aperture. Based on the theoretical estimation of the IR intensity of 3×10^{11} W/cm^2 for the data-set 1 (black circles), the IR intensities used in the successive measurements have been estimated by linear interpolation.
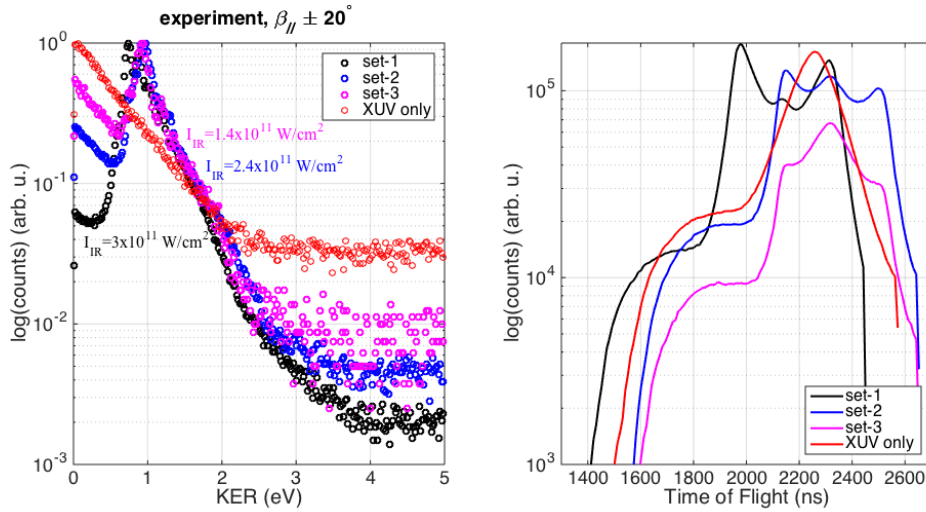
Figure 2: IR fluence estimation. a) Ion fragments (H$^+$ + H) counts in logarithmic scale as a function of their kinetic energy or KER, for four different data sets. The red data-set corresponds to a XUV-only measurement while the others (black, blue and pink) are always XUV+IR each with a different IR intensity. b) H$^+$ ion fragments yield (logarithmic scale) as a function of the time of flight (ns) for the same data sets shown in panel a).

4. Time of Flight (TOF) of the ion fragments
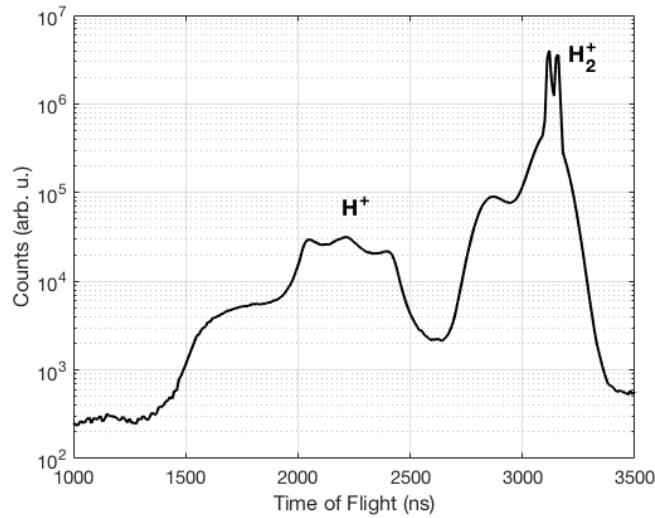
Figure 3: Ion (fragment) TOF. Counts (logarithmic scale) of the collected ions as a function of the TOF showing the H^+ and H_2^+ particles. The H_2^+ ion has a yield of two orders of magnitude higher than the H^+.

5. Theoretical description of the attosecond pulse train and the infrared field.

The IR field is defined as a 3-cycle sine-squared pulse of wavelength 775 nm and peak intensity 3×10^{11} W/cm^2. The attosecond pulse train is theoretically simulated by using a sequence of four single attosecond pulses of 500 as duration (total duration) with a central frequency corresponding to the 17th harmonic of the 775 nm IR field, i.e. $\omega_0 = 27.2$ eV. We use the same maximum peak intensity for each pulse, $I = 10^9$ W/cm^2. The associated vector potential, A(t), is shown in figure 4 together with the IR probe pulse. Positive time delays indicate that the IR field comes after the APT, while negative time delays indicate the other way around.
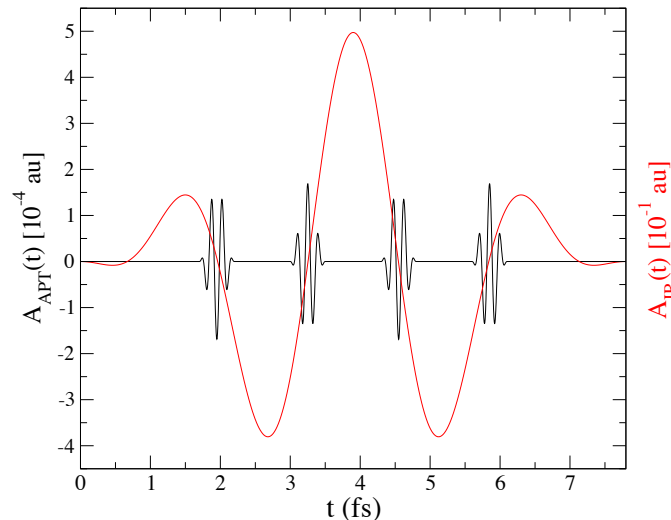
Figure 4: Vector potential for the APT (black) and the IR field (red), for zero time delay between them.

3

6. COLTRIMs ion-detector resolution and calibration

From a He test measurement we could retrieve the temporal resolution of the ion-detector of our COLTRIMs.

When He gas is photoionized by a train of attosecond pulses presenting discrete harmonics centered at discrete photon energies $n\hbar\omega_{IR}$ with $n=$ odd numbers, the He^+ time-of-flight (TOF) spectrum is modulated not only by two peaks corresponding to the ions ejected towards and away from the ion-detector, but also by different peaks due to the different ionizing harmonics, as can be observed in Fig. 5.

We estimate the TOF-resolution of our ion-detector by considering the minimum resolvable distance between two consecutive peaks measured when applying the maximum supported an accelerating electric field of about 25 V/cm. The minimum separation in this configuration results in $\Delta_{TOF}\sim 1.4$ ns.

Please note that in the experimental configuration as described in the main text, the extraction field was more than 5 times weaker (4.4 V/cm), thus making the separation of the ion peaks larger.
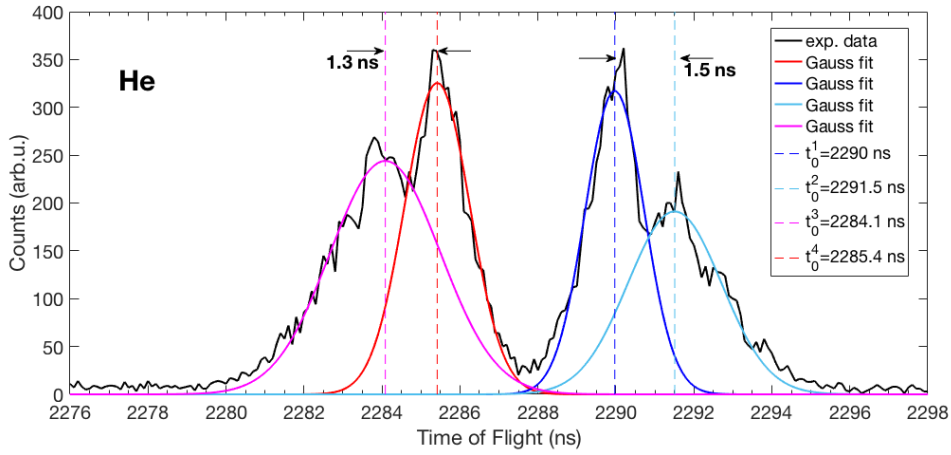
Figure 5: Time-of-flight (**TOF**) resolution. Measured He TOF spectrum (black curve), and two Gaussian fit functions (blue and red solid curves) indicating the peak position of each Gaussian-fit (dashed lines). The applied electric field in this measurement is ~25 V/cm.

On the other hand, for the spatial resolution we considered the distance between two consecutive features composing the observable grid in Fig. 6, which is the ion-detector delay-line. The spatial resolution results approximately $\Delta_{X-Y}\sim 250$ μm (see projection, Fig. 6).
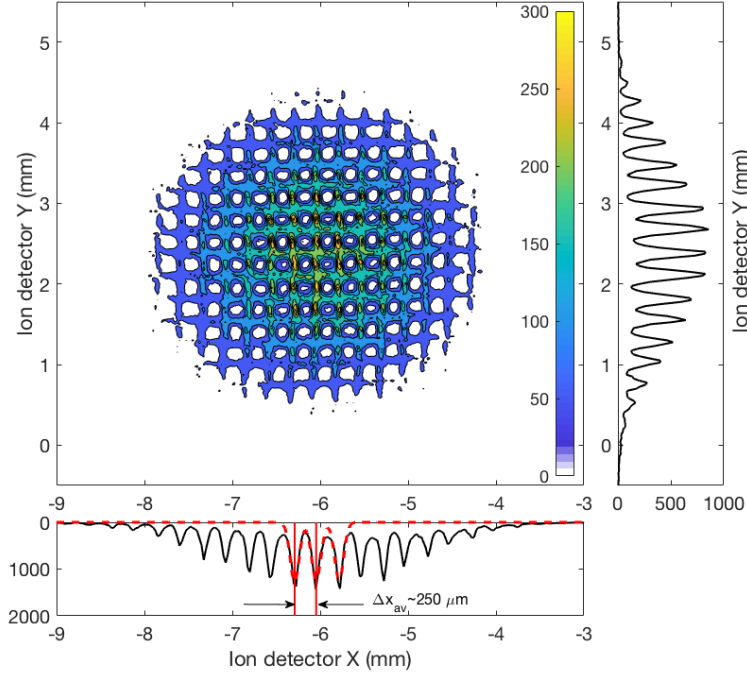
Figure 6: Ion-detector spatial resolution. 2D depiction of the He ion counts (colorbar) as a function of the x and y coordinate of the ion detector (mm). The right and bottom black curves represent the projections of a slices in x (bottom) and y (right) of the 2D image. The red curve on the bottom is a fit function of three Gaussian peaks highlighting the distance between two consecutive peaks of ~250 μm. The electric field applied in this measurement was approx. ~4.4 V/cm.

These two quantities will determine the energy resolution of the kinetic energy release of the collected ion-fragments of the reaction under investigation, i.e. in this work the photodissociation of $H_2 \rightarrow H^+ + H + e^-$.

The following equations have been used to define the x-, y-, z-momenta of the measured ion-fragment H^+:

$$Ip_z = -SI2au \cdot \left(\frac{L \cdot m_{H^+}}{(t - t_0)_{H^+}} - \frac{1}{2} q \cdot E \cdot (t - t_0)_{H^+} \right)$$

$$Ip_x = SI2au \cdot m_{H^+} \cdot \frac{X - X_0}{(t - t_0)_{H^+}}$$

$$Ip_y = SI2au \cdot m_{H^+} \cdot \frac{Y - Y_0}{(t - t_0)_{H^+}}$$

where z is TOF axis while x and y are the two axis on the detector plane, SI2au is the conversion factor from SI units to atomic units (a.u.) of momentum, t is the TOF corrected by a t_0 used to calibrate the detector in order to have the Ip_z momentum centered at 0 a.u., L is the distance over which the ions of charge q and mass m_{H^+} travel accelerated by the electric field E, X and Y indicate the position on the detector corrected by X_0 and Y_0.

The calibration of the electric field E and the t_0 parameter is based on the TOF measurement as expressed in the following formula:

$$TOF(i) = t_0 + \sqrt{\frac{2L}{QE}} \cdot \sqrt{m}$$

5

where i is a specific ion species and m and Q their mass and charge, respectively.

The following parameters: L, X_0 and Y_0 are, on the other hand, results from the calibration of the electron kinetic energy as a function of the α angle (Fig. c-a and d-a), defined as:

$$\alpha = \tan^{-1}\left(\frac{\sqrt{Ep_x^2 + Ep_y^2}}{Ep_z}\right)$$

where $Ep_{x,y,z}$ are the electron momenta in the three directions.

Usually the first calibration is performed on He target gas as shown in Fig. 7. Figure 7-a represents the electron kinetic energy vs. α. Since in this test experiment both XUV and IR are present, not only the mainbands (single XUV photon absorption) can be observed but also of the sidebands (XUV+IR signal). Fig. 7-b shows the electron momentum Ep_y vs. Ep_z, where the z-direction is the TOF axis. Fig 7-c compares the photoelectron spectrum and the XUV photon spectrum shifted by the He ionization potential which is 24.58 eV. The match is obtained by multiplying the Ep_z momentum by a specific scaling factor. Consequently also the Ip_z momentum will be multiplied by the same scaling factor. Figs. 7-e and 7-f represent the ion momenta Ip_y vs. Ip_z and Ip_y vs. Ip_x, respectively. The white dot indicates the (0,0) coordinate. Figure 7-d represents the momentum sum ion+electron for the three coordinates which must be centered at 0 a.u.. The parameters extracted from the He calibration will be used as a first guess for calibrating the H_2^+ and the H^+ ionic fragments.
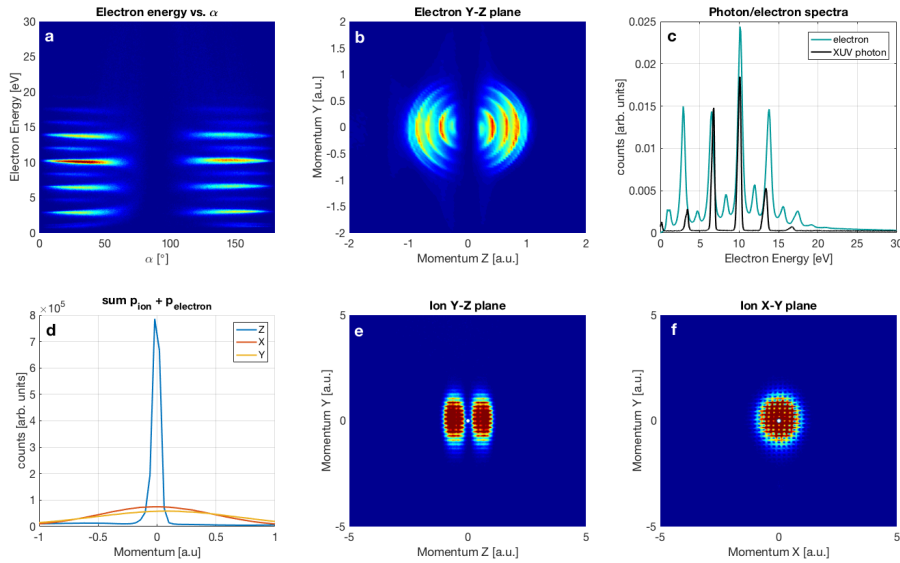
Figure 7: He calibration test measurement. Calibration of ion-electron detectors for He photoionization test measurement (XUV+IR): a) Experimental electron kinetic energy as a function of the α angle. b) Electron momenta Ep_y vs Ep_z in a. u.. c) Comparison between the photoelectron spectrum and the photon XUV spectrum shifted by the He ionization potential. d) Momentum sum ion + electron. e) and f) ion momenta Ip_y vs Ip_z and Ip_y vs Ip_x, respectively.

Figure 8 is the equivalent of Fig. 7 but for the $H^+ + H + e$ reaction. In this case the electron kinetic energy must be considered together with the nuclear fragments kinetic energy called kinetic energy release (KER) to be compared with the XUV photon shifted by the H_2^+ dissociation limit of 18.08 eV. In Figs. 8-a and 8-b it has been

operated an α selection of 60 deg (electrons detection cone), as mentioned in the main text. The calibration of the electron and ion detectors, in case of a multi-ion reaction, needs to satisfy the conservation energy condition not only looking at Fig. 8-c but also at the 2D correlation diagram between electron kinetic energy and KER, which defines a unique reaction path for each dissociating molecule, as shown in Fig 2 in the main text and Fig. 1.
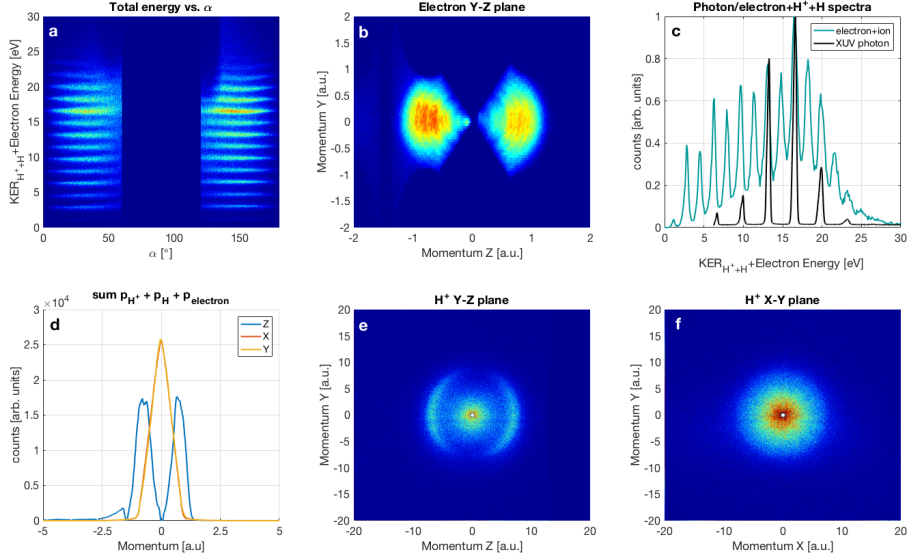
Figure 8: H⁺ calibration measurement. Calibration of ion-electron detectors for H⁺+H+e dissociative photoionization measurement (XUV+IR): a) Experimental total energy (KER+electron kinetic energy) as a function of the α angle selected over a cone from 0 to 60 and from 120 to 180 degrees. b) Electron momenta Ep_y vs Ep_z in a. u. with the same α-cone selection. c) Comparison between the photoelectron+ion energy spectrum and the photon XUV spectrum shifted by the H_2^+ dissociation limit of 18.08 eV. d) Momentum sum ion + neural+electron. e) and f) H⁺ ion momenta Ip_y vs Ip_z and Ip_y vs Ip_x , respectively.

The proton kinetic energy has been defined as follows:

$$K_{H^+} = \text{au2eV} \cdot m_e \frac{(Ip_x^2 + Ip_y^2 + Ip_z^2)}{m_{H^+}}$$

where au2eV is the conversion factor from a.u. to eV, and we obtain an upper limit for the energy resolution of about 0.09 eV for the case of H_2 molecule. On the other hand, additional measurements on different target molecules (not shown here) allow us to estimate a higher energy resolution for our ion detector in the range of about 0.05 eV.